



Cu, Fe and Mn oxides intercalated SiO₂ pillared magadiite and ilerite catalysts for NO decomposition

Katabathini Narasimharao^{a,*}, Islam Hamdy Abd El Maksod^{a,b}, Mohamed Mokhtar^{a,b,*}

^a Surface Chemistry and Catalytic Studies (SCCS) Group, Department of Chemistry, Faculty of Science, King Abdulaziz University, P. O. Box 80203, Jeddah, 21589, Saudi Arabia

^b Physical Chemistry Department, National Research Centre, Dokki, Cairo, 12622, Egypt

ARTICLE INFO

Keywords:

SiO₂ pillared silicates
Magadiite
Ilerite
Cu, Fe, Mn oxides
NO decomposition

ABSTRACT

Synthesized magadiite and ilerite samples were pillared with SiO₂ and then intercalated with Cu, Fe and Mn oxides to utilize for direct NO decomposition between 400 and 600 °C. Cu-SiO₂-pil-ile and Cu-SiO₂-pil-mag catalysts exhibited high NO decomposition activity compared to Fe and Mn oxide intercalated catalysts. Remarkably, Cu-SiO₂-pil-ile offered 90 % NO conversion and 83 % N₂ selectivity at 600 °C. Elemental analysis, XRD, FESEM, DR UV-vis, Raman spectroscopy, N₂-adsorption, H₂-TPR, O₂-TPD and XPS were utilized to study physicochemical characteristics of the materials. The results from XRD and N₂ adsorption demonstrated that the samples possessed different pore structures from SiO₂-pillared silicates, due to different nature of metal oxides. The Cu-SiO₂-pil-ile and Cu-SiO₂-pil-mag samples possess a smaller number of Lewis and Brønsted acid sites compared with Fe and Mn oxide intercalated samples. Presence of Cu²⁺/Cu⁺ and Fe³⁺/Fe²⁺, and synergism between redox centers are major reason for superior performance in NO decomposition. Therefore, the impact of redox properties and NO adsorption on the surface of the catalyst are significant.

1. Introduction

Some of the emission gases such as nitrogen monoxide (NO), nitrogen dioxide (NO₂), sulfur dioxide (SO₂) and carbon monoxide (CO) are considered as indirect greenhouse gases [1], while carbon dioxide (CO₂), nitrous oxide (N₂O), and methane (CH₄) are designated as the direct greenhouse gases [2]. The direct NO decomposition is the best suitable approach for NO removal due to its simplicity [3]. The direct NO decomposition is thermodynamically favorable at temperatures below 1700 °C, however the rate of the reaction is low [4]. The catalytic decomposition of NO is well studied due to the fact that it is recognized as the suitable process for NO elimination from exhaust streams [5]. The two major issues those need to be addressed for development of NO decomposition catalyst are catalyst activity and durability [4,5]. The design and development of an effective heterogeneous catalyst for direct NO decomposition would eliminate the utilization of different types of reducing agents. This process could greatly help to simplify the process of elimination of NO and decreases the cost of NO control in different industrial sectors [6].

A variety of catalysts were utilized for the decomposition of NO gas,

including noble metals [7], metal oxides [8] and ion exchanged zeolites [9]. Noble metals such as Rh and Pd were proved as an active species in three-way catalytic converters; these catalytic systems exhibited superior performance for the NO decomposition [1]. However, the catalysts containing noble metals are expensive and unstable at high temperature as well as the catalysts which contained noble metals deactivate quickly in the presence of oxygen [10]. Transition metal oxides (e.g. Co, Cu, Fe and Mn oxides) based catalysts were also exhibited better catalytic activities for NO decomposition due to their superior redox behavior [11]. Utilization of the transition metal oxides is highly explored due to their high abundance in nature and inexpensive. It was also observed that the transition metal ion exchanged mesoporous zeolites, primarily Cu-exchanged ZSM-5 materials were good catalysts for NO decomposition [12]. However, several tests with the transition metals contained zeolite catalysts had demonstrated that zeolites inefficiently catalyze NO decomposition [13]; the catalysts were oxidized when the reaction progresses and finally the NO decomposition was inhibited. Moreover, the zeolite materials are suffering from a major limitation that they are not hydrothermally stable [14].

Interestingly, in the layered silicates, the distance between silica

* Corresponding authors at: Surface Chemistry and Catalytic Studies (SCCS) Group, Department of Chemistry, Faculty of Science, King Abdulaziz University, P. O. Box 80203, Jeddah, 21589, Saudi Arabia.

E-mail addresses: nkatabathini@kau.edu.sa (N. Katabathini), mmoustafa@kau.edu.sa (M. Mokhtar).

<https://doi.org/10.1016/j.apcata.2021.118100>

Received 18 November 2020; Received in revised form 7 March 2021; Accepted 10 March 2021

Available online 15 March 2021

0926-860X/© 2021 Elsevier B.V. All rights reserved.

layers can be adjusted by swelling and pillaring, thereby enabling the large molecules to diffuse to reach active centers located in between the layers; this unique property provides layered silicates a significant advantage over the microporous zeolites [15]. The synthesis of pillared layered silicates expanded considerably due to the scope of their utilization as heterogeneous catalysts for different chemical reactions [16]. It was observed that layered materials pillared with inorganic oxides possessed meso/macro pore structure, high thermal stability and high surface area as similar as meso porous zeolites [17]. Synthetic layered silicates such as magadiite ($\text{Na}_2\text{Si}_4\text{O}_{29}\cdot x\text{H}_2\text{O}$) and ilerite ($\text{Na}_2\text{Si}_8\text{O}_{17}\cdot x\text{H}_2\text{O}$) are considered to be useful hosts for many pillared materials [18]. These materials possessed similar characteristics as natural clay materials and the interlayer spaces could be expanded simply by intercalation of guest molecules in the layers. Several years ago, Landis et al. [19] synthesized high surface area contained SiO_2 -pillared magadiite (around $530\text{ m}^2\text{ g}^{-1}$) by reacting the tetraethyl orthosilicate with octylamine. Later, Kosuge and Tsunashima [20] reported the preparation of very high surface area ($1000\text{ m}^2\text{ g}^{-1}$) containing silica-pillared ilerite by intercalation of octylamine and tetraethyl orthosilicate into the layered ilerite. In the past, Schwieger et al. synthesized Pt ion exchanged ilerite silicate using $\text{Pt}(\text{NH}_3)_4^{2+}$ as Pt precursor and observed that Pt loaded ilerite materials exhibited bifunctional character [21,22]. Schwieger et al. also synthesized Pt loaded magadiite materials and observed that the structure of the silica layers was not affected even after 22.2 wt% Pt loading [23]. Kim et al. [24] prepared and characterized metal (Ti, Fe, Zr) oxide pillared layered ilerite samples. Introduction of transition metals such as Cu, Fe and Mn could generate redox active sites, which enhance the activity of layered silicate materials for redox type reactions [25]. Ahn et al. [26] synthesized Cu, Zn - pillared ilerite materials and used as catalysts for direct synthesis of dimethyl ether from synthesis gas. Ozawa et al. [27] synthesized well dispersed Ag and ZnO magadiite nanocomposites with size between 3–5 nm. However, synthesis and application of manganese oxide-pillared layered silicates were not reported well in the literature [28].

Ding et al. [29] reviewed the catalytic activities of different pillared silicates for the selective catalytic reduction (SCR) of NO with NH_3 . It was observed that the pillared layered silicate catalysts were stable in presence of SO_2 and H_2O and exhibited higher activity compared to conventional vanadium-titanium oxide catalysts. Although, the NH_3 -SCR and direct NO_x decomposition processes follow different reaction mechanisms, the transition metal oxide contained pillared layered silicates could be better catalysts for direct NO decomposition [30]. In the present work, magadiite and ilerite were first pillared with SiO_2 and then intercalated with Cu, Fe and Mn oxides. The synthesized materials were utilized for direct NO decomposition and also analyzed by different characterization techniques to study their physico-chemical properties. The role of structural and electronic properties of the materials with NO decomposition activity was established.

2. Experimental

2.1. Synthesis of magadiite and ilerite materials

The synthesis procedure of Na-magadiite is described as reported in the literature [23]. The synthesis solution was prepared by mixing the Si and Na precursors containing known amount of water (a weak alkaline and SiO_2 -rich ternary system with $\text{SiO}_2\text{:Na}_2\text{O:H}_2\text{O}$ molar ratio of 5:1:75). Afterwards, Na_2CO_3 was added in small portions, until a dense gel was formed (pH~12.5). A hydrothermal method at $140\text{ }^\circ\text{C}$ for 48 h was used to crystallize the Na-magadiite sample. Then the obtained solid sample was filtered and washed and dried at $110\text{ }^\circ\text{C}$ for 12 h. The preparation procedure to synthesize sodium form of ilerite is similar same as that described by Kärger et al [31]. Na-ilerite was synthesized using colloidal silica (Ludox AS-40), sodium hydroxide pellets and deionized water as starting materials for the preparation of the synthesis gel. The obtained synthesis gel was directly transferred into the

autoclave without aging. The synthesis temperature was set as $100\text{ }^\circ\text{C}$ and the crystallization was carried out for 21 days under static conditions.

2.2. Post-synthetic modifications

2.2.1. Swelling of silicates with hexadecyltrimethylammonium bromide (CTAB)

In the first step of post-modification, the layered silicates (magadiite and ilerite) were swollen with quaternary ammonium surfactant, CTAB ($\text{C}_{19}\text{H}_{42}\text{BrN}$) at $40\text{ }^\circ\text{C}$ under high pH conditions (pH~14). Typically, 9.0 g of aqueous clay slurry (20 wt. % solid) was added to 35.0 g of an aqueous solution of 29 wt. % of CTAB and 11.0 g of an aqueous solution of 40 wt. % tetrapropyl ammonium hydroxide (TPAOH). The mixture was then stirred for 24 h at $40\text{ }^\circ\text{C}$.

2.2.2. Pillaring with SiO_2

The materials after swelling procedure were recovered by repetitive cycles of centrifugation and washed with deionized water, then dried at $75\text{ }^\circ\text{C}$ for 12 h. Typically, 1.0 g of swollen silicate was mixed with 5.0 g of tetraethyl orthosilicate and stirred for at $80\text{ }^\circ\text{C}$ for 24 h. Finally, the impregnated product was filtered and dried at $30\text{ }^\circ\text{C}$ for 12 h to remove the excess silica from the solid surface. Then, a known amount (1.0 g) of dried impregnated solid was hydrolyzed with 10 g of water for at $40\text{ }^\circ\text{C}$ for 5 h. Then, the hydrolyzed product was filtrated and washed with deionized water. Finally, the filtered cake was dried at $75\text{ }^\circ\text{C}$ for 12 h and calcined at $600\text{ }^\circ\text{C}$ for 5 h under air flow (120 mL min^{-1}) in a muffle furnace with a heating rate of $1.0\text{ }^\circ\text{C min}^{-1}$.

2.3. Intercalation of pillared silicates with Cu, Fe and Mn oxides

To synthesize the catalytically active pillared layered silicates, transition metal (Cu, Fe and Mn, 15 wt.%) oxides were intercalated with pillared layered silicates. Typically, calculated amount of metal oxide precursor [$\text{Cu}(\text{NO}_3)_2\cdot 3\text{H}_2\text{O}$ or $\text{Fe}(\text{NO}_3)_3\cdot 9\text{H}_2\text{O}$ or $\text{Mn}(\text{NO}_3)_2\cdot 4\text{H}_2\text{O}$] was dissolved in deionized water and the pillared layered silicate containing the same volume was added under constant stirring. Then, the excess water was removed in vacuum oven and the dried powders were thermally treated at $600\text{ }^\circ\text{C}$ for 4 h in the air under static conditions to obtain the final catalysts.

2.4. Characterization of materials

The chemical composition (atomic ratios of elements) of the samples was measured by using Perkin-Elmer ICP-AES instrument. The XRD patterns of the samples were recorded using Bruker D8 Advance X-ray diffractometer using Ni filtered Cu $K\alpha$ radiation ($\lambda = 1.5405\text{ \AA}$). The FE-SEM analysis of the samples was carried out using JEOL Model JSM-6390LV microscope. The N_2 physisorption measurements were carried out using Quantachrome Autosorb ASIQ instrument at liquid nitrogen temperature. The DR UV-vis analysis of the samples was performing using Thermo-Scientific evolution spectrophotometer in the wavelength range of 220–1000 nm. The Raman spectra of the synthesized samples were obtained using Bruker Equinox 55 FT-IR spectrometer. The XPS spectra of samples were obtained using a SPECS GmbH X-ray photoelectron spectrometer. The H_2 -TPR and O_2 -TPD analyses of the synthesized samples were carried out using Quantachrome CHEMBET-3000 instrument [32]. DRIFT spectra of pyridine adsorbed samples were obtained to determine the acidic properties of the synthesized samples. The detailed experimental procedures are provided in the electronic supplementary information (ESI).

2.5. Catalytic NO decomposition

Catalytic direct NO decomposition reactions over synthesized catalysts were performed using a quartz micro reactor (id of 80 mm) at

atmospheric pressure. Calculated amount (0.1 g) of sieved catalyst particles loaded into the quartz reactor. The reactor consisted of a quartz frit support and the catalyst particles (grain size of 60–80 μm , volume of the catalyst bed is 0.5 cm^3) was placed on the frit, and covered with a layer of quartz wool and the catalyst was thermally treated at 600 $^\circ\text{C}$ in flow of helium gas before start of the reaction. The catalytic performance was evaluated using 0.1 vol.% NO balanced by helium gas (total flow of the gas is 200 mL min^{-1}) at temperature range of 400–600 $^\circ\text{C}$. The NO concentration was continuously monitored by a chemiluminescent NO/ NO_x analyzer (Thermo Electron Corporation, model 10). A Shimadzu GC model 14A was used to analyze the concentrations of N_2 and N_2O in the product stream. The analytical system had two capillary columns: a Poropak-Q column used to analyze N_2O and a molecular sieve SA used to analyze N_2 , O_2 , and NO. The NO conversion, N_2 yield and rate of N_2 formation were evaluated with every 50 $^\circ\text{C}$ increment. The reaction was carried out at each temperature for at least 30 min. to allow reaction to reach steady state. The NO conversion and N_2 selectivity were calculated using the following equations.

$$\text{NO conversion (\%)} = \{[\text{NO}]_{\text{inlet}} - [\text{NO}]_{\text{outlet}} / [\text{NO}]_{\text{inlet}}\} \times 100 \quad (1)$$

$$\text{N}_2 \text{ selectivity (\%)} = \{[\text{NO}]_{\text{inlet}} - [\text{NO}]_{\text{outlet}} - [\text{NO}_2]_{\text{outlet}} - [\text{N}_2\text{O}]_{\text{outlet}} / [\text{NO}]_{\text{inlet}} - [\text{NO}]_{\text{outlet}}\} \times 100 \quad (2)$$

$[\text{NO}]_{\text{inlet}}$ = concentration of NO in the inlet, $[\text{NO}]_{\text{outlet}}$ = concentration of NO in the outlet, $[\text{N}_2\text{O}]_{\text{outlet}}$ = concentration of N_2O in the outlet, $[\text{NO}_2]_{\text{outlet}}$ = concentration of NO_2 in the outlet

3. Results and discussion

The powder X-ray diffraction patterns for as-synthesized Na-magadiite and Na-ilerite samples are shown in Fig. S1 (ESI). The Na-magadiite sample displayed characteristic reflections of well-defined magadiite at $2\theta = 5.7^\circ$, 11.3° , 17.11° corresponding to the (001), (002), and (003) crystalline planes, respectively as per JCPDS 42–1350 [33]. The reflections found between 23° and 30° are revealing the

presence of magadiite phase in the sample. The 2θ positions for characteristic reflections for Na-ilerite structure are clearly observed at 8.0° , 18.6° , 21.8° , 25.6° , 29.2° in the X-ray pattern for as-synthesized Na-ilerite sample and these findings are in excellent agreement with cited literature [31]. No additional reflections for any other phases were detected in the XRD patterns of Na-magadiite and Na-ilerite samples indicating the effective synthesis of the layered silicates.

Presence of (00 L) reflection corresponding to the basal spacing, $d_{(001)}$ after swelling and pillaring of layered silicates with CTAB and SiO_2 can be clearly observed (electronic supplementary information, ESI). The basal spacing corresponding to the $d_{(001)}$ reflection was calculated for both the samples and it was observed that the SiO_2 pillared magadiite and ilerite samples possessed basal spacing of 1.54 nm and 1.11 nm respectively and these values are in accordance with the previously reported results [34]. Fig. 1 (A) & (B) shows the XRD patterns for the Cu, Fe and Mn oxides intercalated SiO_2 -pillared magadiite (A), ilerite (B) samples. These samples show dissimilar XRD patterns from Na-magadiite and Na-ilerite samples due to SiO_2 pillaring and intercalation of metal oxide between the layers of silicates. The XRD patterns of the samples are clearly exhibiting the presence of broad reflection in the range of $2\theta = 15\text{--}33^\circ$, which could be attributed to the amorphous SiO_2 as it forms as a pillar between the interlayers of silicates. The pillared structures are found to be created by the intercalation of SiO_2 between the silicate layers for each calcined product [35]. It was reported that transition metal oxides could form due to the decomposition of metal hydroxide, which formed by metal ions reacting with the $-\text{OH}$ groups intercalated between the layers [36]. There is another clear possibility for the reaction between the SiO_2 and metal precursors to form amorphous metal silicates.

The XRD patterns of Cu oxide intercalated magadiite and ilerite samples exhibited sharp reflections at 35.4° , 38.4° and 48.9° due to (110), (002) and (111) planes of the monoclinic phase of CuO (crystalite size of 20 nm) [JCPDS#45–0937]. Lim et al. [37] observed the appearance of reflections due to copper hydroxide phase in case of Cu oxide intercalated magadiite sample. The Fe intercalated magadiite and

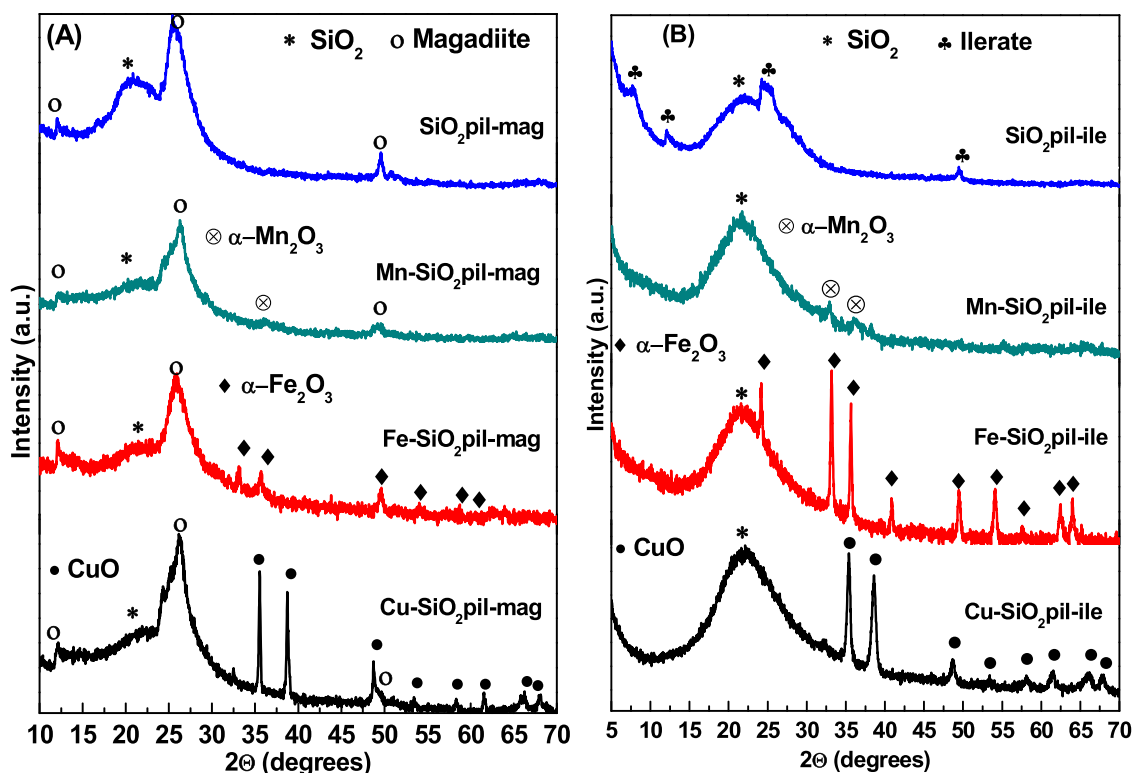


Fig. 1. Powder XRD patterns of Cu, Fe and Mn oxides intercalated SiO_2 -pillared (A) magadiite (B) ilerite samples.

ilerite samples also showed the reflections due to presence of pure $\alpha\text{-Fe}_2\text{O}_3$ phase [JCPDS#24-0072] with rhombohedral structure. The presence of highly intense reflections due to CuO and $\alpha\text{-Fe}_2\text{O}_3$ phases is an evidence for the formation of aggregated CuO and $\alpha\text{-Fe}_2\text{O}_3$ particles

on the external surface of the SiO_2 pillared ilerite. Interestingly, the XRD patterns of Mn oxide intercalated magadiite and ilerite samples exhibits low intense reflections at 32.95° and 38.23° corresponding to (222) and (440) planes of $\alpha\text{-Mn}_2\text{O}_3$ [JCPDS 41-1442]. Presence of low intense

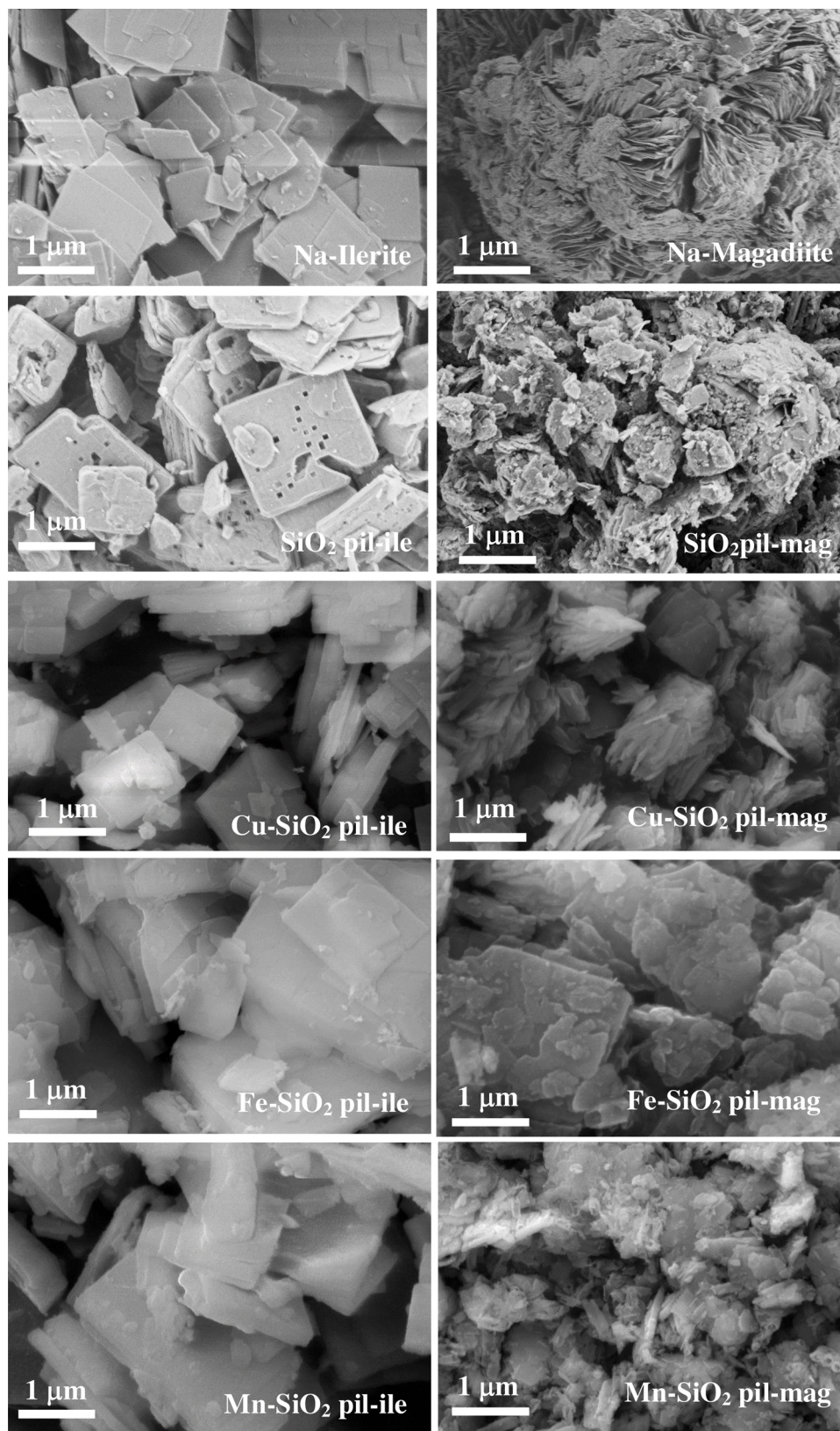


Fig. 2. FE-SEM images of Cu, Fe and Mn oxides intercalated SiO_2 -pillared magadiite and ilerite samples.

reflections could be due to the fact that the formed α - Mn_2O_3 was in a small size, and any bulk aggregation was not occurred. In this study, Cu, Fe and Mn oxides intercalated SiO_2 pillared magadiite and ilerite samples were calcined at 550°C and the samples still exhibited the ordered basal spacing, proving that the expanded galleries did not collapsed after removal of CTAB. This observation revealing that the synthesis procedure used in this study are suitable for the formation of strong metal oxide pillars. It is well known that the 2θ values of $d_{(001)}$ reflections reveal the extent of layer expansion due to metal oxide pillaring, and the expansion levels are different with type of pillared oxide. The XRD analysis results are also indicating that Cu, Fe and Mn oxides intercalated SiO_2 pillared magadiite and ilerite samples shows increase in the basal spacing. The values are higher (1–2 nm) compared to SiO_2 pillared magadiite and ilerite samples reported in the literature [35]. This behavior is probably due to the presence of large hydrated Cu, Fe and Mn oxides, confirming the intercalation of the metal oxides between the silicate layers.

Fig. 2 shows FE-SEM images for all the synthesized samples including Cu, Fe and Mn oxides intercalated SiO_2 pillared ilerite and magadiite samples. It was previously reported that natural magadiite sample possesses thin sheet-like morphology, however, synthetic magadiite samples normally exists in rosette-like shaped crystals [38]. Contrary to synthesized magadiite morphology, the synthetic ilerite crystals shows plate-like morphology [39]. It is clear from the FE-SEM images that Na-magadiite and Na-ilerite samples exhibited morphology as previously reported. It is clear that thin rectangular plate shaped Na-ilerite crystallites were preserved even after swelling with CTAB, SiO_2 pillaring and calcination at 600°C . The crystallites of the Cu, Fe and Mn intercalated SiO_2 -pillared ilerite samples exhibited a similar morphology as as the Na-ilerite shape. Metal oxide modified SiO_2 pillared ilerite samples consisted of relatively large agglomerates of irregular and rectangular plate-shape crystals typical for the ilerite phase.

The typical ilerite thin plate shape structure was still preserved after metal oxide intercalation as shown in SEM images. The SiO_2 pillared magadiite sample exhibited small separated rosette-shaped islands with quite large interparticle spaces. The diameter for “flower” and “petals” were reduced to about 0.5–1.0 μm . The observed suppression in particle size and creation of interparticle spaces could enhance the surface area and the mesoporous nature of pillared samples. The subsequent impregnation of Cu and Fe oxides over SiO_2 pillared magadiite led to change of morphology to sheet like crystals, with sharp edges fairly defined [40]. Interestingly, the Mn modified SiO_2 pillared magadiite sample showed a similar morphology as the SiO_2 pillared magadiite sample. Only small amounts of rosettes-shaped crystals, confirming

existence of the magadiite phase, were detected. This sample consisted of agglomerates of rosette-shaped crystals with amorphous material present on their surface, which correlates very well with the XRD results.

The DR UV-vis absorption spectra of synthesized samples are shown in Fig. 3. It is clear from the figure that all SiO_2 pillared magadiite and ilerite samples displayed absorption band centered at 247 nm. Chen et al. [41] reported that the layered silicate sample exhibits a large absorption band in the range of 200–300 nm with a shoulder around 250 nm attributed to silica wavelength region. As anticipated, the metal oxide intercalated SiO_2 pillared magadiite and ilerite samples exhibited additional UV-vis absorption bands. The Cu- SiO_2 -pillar-mag and Cu- SiO_2 -pillar-ile samples showed a broad band in between 400 nm and 850 nm, which could be attributed to d - d transition of Cu^{2+} species [42]. The appearance of pronounced asymmetric peak shape suggests that the formed copper oxide have different size distribution broad peak which could be attributed to the presences of copper oxide nanoparticles [43].

The DR UV-vis spectra for Fe- SiO_2 -pillar-mag and Fe- SiO_2 -pillar-ile samples shows absorption peaks due to presence of different Fe (III) species. It is known that O-Fe charge transfer transitions generally appears at 240–300 nm and peaks in the region of 400–600 nm could be ascribed to the d - d electron pair transition in isolated Fe(III) species. The peaks appears beyond 500 nm could be attributed to large iron oxide particles [44]. The Fe- SiO_2 -pillar-mag and Fe- SiO_2 -pillar-ile samples show broad absorption peak at the range of 400–600 nm. It can be observed that the peak maximum for magadiite is at wavelength of 460 nm. The center of absorbance peak for Fe- SiO_2 -pillar-ile sample was at the wavelength around 520 nm. It was previously reported that the absorbance peak shifts towards a higher wavelength with increase in the particle size [45]. The peak identified around 900 nm in both the samples is due to the quantum size effect of α - Fe_2O_3 nanoparticle structure [46] and the size of the iron oxide particles were more in case of ilerite compared to magadiite. The DR UV-vis absorption spectra of Mn- SiO_2 -pillar-mag and Mn- SiO_2 -pillar-ile samples exhibited broad absorption peaks at 390 and 400 nm, respectively. It was previously reported that layer structured manganese oxide materials exhibit UV-vis absorption peak centered on 380 nm [47]. The broad band at 400 nm with a tail extending to 900 nm in both the samples, this is possibly due to the presence of isolated Mn oxide clusters on the external surface of the layered silicates. A similar observation was previously reported in case of Mn exchanged zeolites [48].

The XPS measurements were used to evaluate the elemental composition and oxidation states of metals presented in the synthesized catalysts. The deconvoluted XP spectra of the synthesized samples are shown in Fig. 4. It is clear from the figure that $\text{Si}2p$ XPS peaks could be deconvoluted into two different peaks at binding energies (BE) of

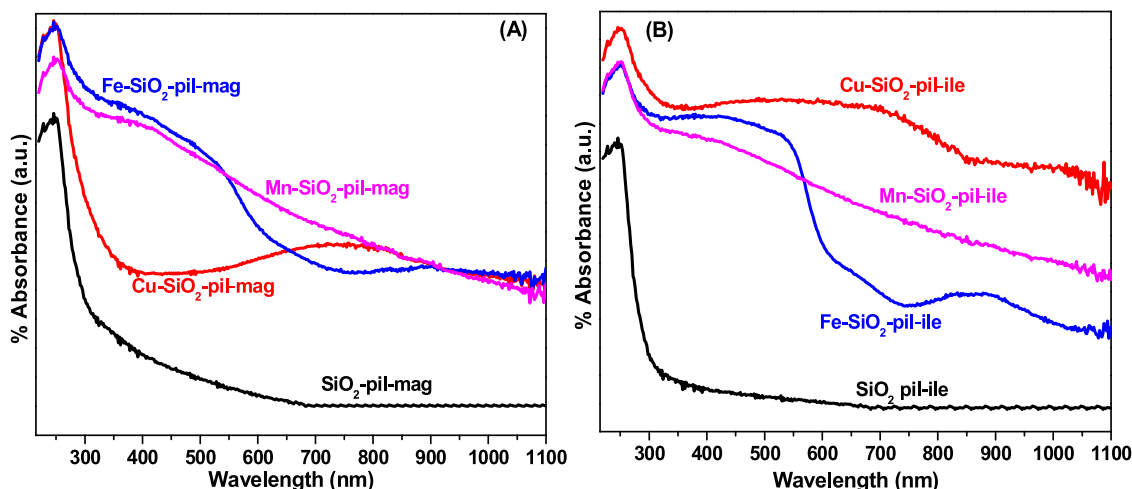


Fig. 3. DR UV-vis spectra of Cu, Fe and Mn oxides intercalated SiO_2 -pillared (A) magadiite and (B) ilerite samples.

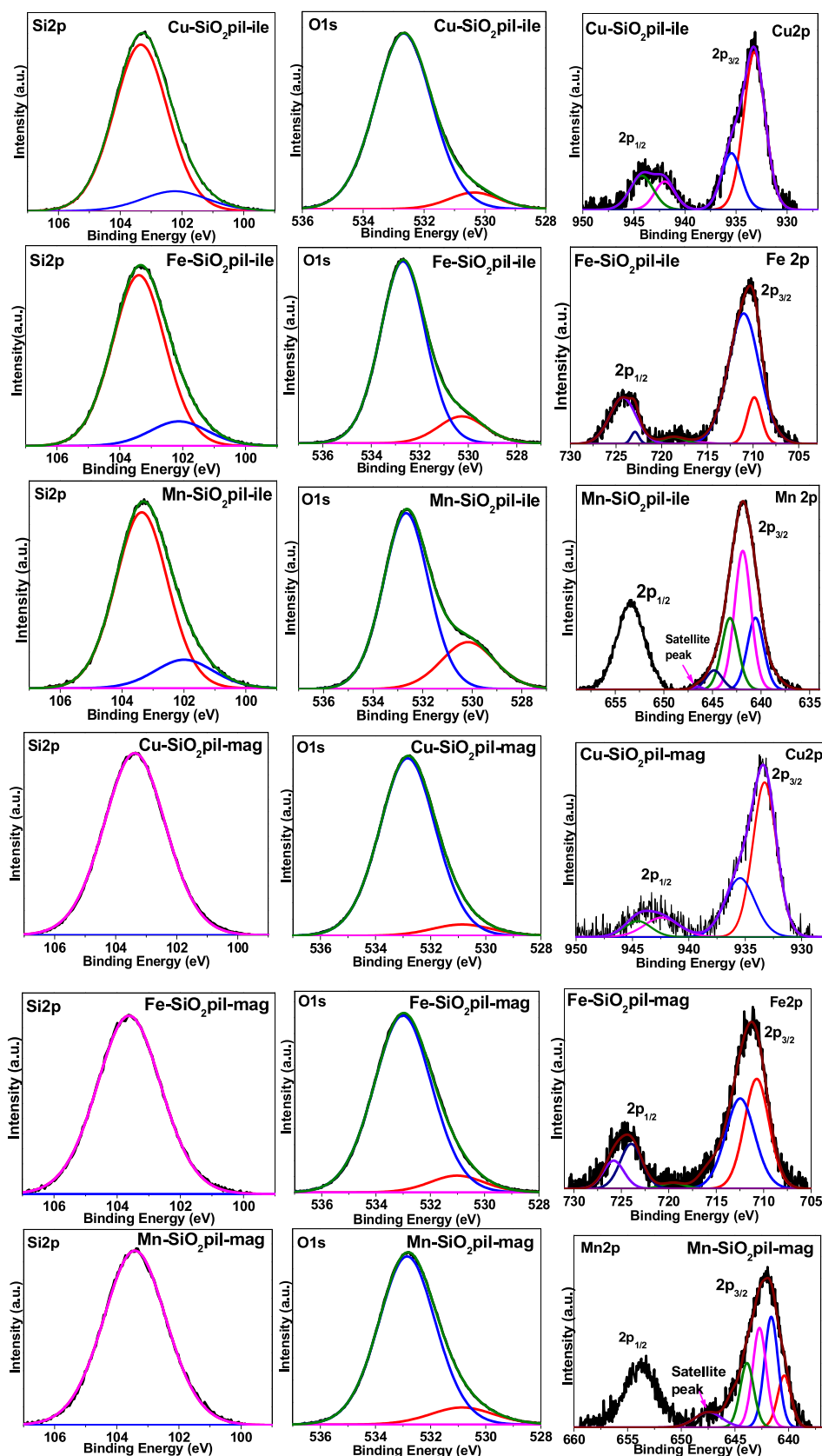


Fig. 4. The deconvoluted XPS spectra of Cu, Fe and Mn oxides intercalated SiO_2 -pillared ilerite and magadiite samples.

103.3 eV and 102.2 eV in all the ilerite samples. It was previously reported that the Si2p peak at 103.3 eV could be attributed to Si in the tetrahedral sites of layer silicate [49] and this peak shifts to lower BE value, when Si atoms are bonded with another metal atoms [50]. Therefore, the minor Si2p peak appeared at 102.2 eV could be assigned to the Si-O-M (M = Cu, Fe and Mn) species presented in the metal intercalated SiO₂ pillared ilerite samples. In contrary, the magadiite samples exhibited a single peak at BE of 103.3 eV corresponding to the Si in tetrahedral sites of layered silicate as bulk magadiite sample (Fig. S2) and absence of Si2p peak at 102.2 eV in these samples reveal that the surface Si species are not in direct contact with metal oxide species in case magadiite samples.

The both Cu oxide intercalated SiO₂ pillared samples exhibited two Cu 2p_{3/2} peaks at 933.1 eV and 935.3 eV. Huang et al. [51] assigned the peak at 933.1 eV for the Cu²⁺ of CuO and the other peak at 935.3 eV for the copper phyllosilicate species. This observation reveal that Cu is chemically bonded with Si-O groups in both ilerite and magadiite samples to form an amorphous copper phyllosilicate phase on the surface. It is clear from the intensity of the peaks that the CuO contribution is more compared to the copper phyllosilicate reveal presence more CuO particles on the surface of the layered silicates. The Fe oxide intercalated SiO₂ pillared ilerite sample exhibited two different Fe 2p_{3/2} peaks; a major peak at BE of 711.1 eV and a minor peak at 709.8 eV. Grosvenor et al. [52] reported that fitting of Fe 2p_{3/2} peak for α-Fe₂O₃ phase yields peaks at 709.4 eV and 711.1 eV for Fe²⁺ and Fe³⁺ species, respectively. Therefore, presence of α-Fe₂O₃ particles (majority Fe³⁺) on the surface of ilerite is evidenced from XPS analysis. On other hand, the Fe oxide intercalated SiO₂ pillared magadiite sample exhibited two equally intense peaks at 710.6 eV and 712.3 eV due to Fe²⁺ and Fe³⁺ species, respectively. The shift in the BE towards higher levels could be attributed to the decrease in the amount of Fe³⁺ species in the α-Fe₂O₃ particles. These observations are in agreement with the XRD results that this sample exhibited low intense XRD reflections due to α-Fe₂O₃ phase.

The deconvoluted Mn2p peaks for the Mn oxide intercalated SiO₂ pillared samples also presented in the Fig. 4. As shown in the figure, Mn2p spectra of the samples were broadened by multiplet splitting, which is due to the coupling between the excited unpaired 2p core-electron and unpaired 3d valence electrons. The deconvoluted Mn2p spectra also includes the shake-up satellite peaks. It was previously reported that Mn 2p_{3/2} spectrum of Mn cations exhibits four major multiplet peaks separated by approximately 1.0 eV [53]. The XPS spectrum of Mn oxide intercalated SiO₂ pillared ilerite sample also showed four Mn 2p_{3/2} peaks at 640.5 eV, 641.9 eV, 643.2 eV and 644.8 eV, with a minor satellite peak. Similarly, Mn oxide intercalated SiO₂ pillared magadiite sample showed four peaks at 640.4 eV, 641.6 eV, 642.7 eV and 643.8 eV along with a major satellite peak. The average BE of the peaks is 642.1 eV and 642.6 eV for ilerite and magadiite samples and this observation indicating that the both samples possessed Mn³⁺ species [54]. In case of Cu, Fe and Mn oxides intercalated SiO₂ pillared ilerite samples, the O1s spectra were deconvoluted into two components at 530.3 eV and 532.7 eV. The lower BE peak could be attributed to metal oxide species and higher BE peak could be assigned to the O₂⁻ species of the silicate layers [55]. The O1s spectra of Cu, Fe and Mn oxides intercalated SiO₂ pillared magadiite samples also exhibited two peaks at 530.8 eV and 532.8 eV corresponding to oxygen species in metal oxide and silicate layers. Slight increase of BE in the magadiite samples is due to the small size particles presented in these samples.

The bulk and surface elemental composition of the synthesized samples were obtained using ICP-AES and XPS techniques. The obtained results are tabulated in Table 1. The bulk composition of the sodium salts of ilerite (Na₂Si₈O₁₇·10H₂O) and magadiite (Na₂Si₁₄O₂₉·83H₂O) samples were quite matching with the idealized formulas proposed in the literature [56]. The bulk chemical composition data obtained for the SiO₂ pillared and metals intercalated pillared ilerite and magadiite samples indicate that all these materials retain the structure of the

Table 1
Elemental analysis of the synthesized samples.

Catalyst	Elemental composition (wt. %)							
	Bulk				Surface			
	Na	Si	O	Metal	Na	Si	O	Metal
Na-mag	4.2	43.5	52.2	–	3.9	43.3	52.5	–
SiO ₂ -pil-mag	1.1	57.4	41.4	–	0.6	41.3	58.1	–
Mn-SiO ₂ -pil-mag	0.2	54.6	33.0	12.2	–	35.4	54.1	10.4
Cu-SiO ₂ -pil-mag	0.1	54.0	33.5	12.4	–	34.9	53.8	11.3
Fe-SiO ₂ -pil-mag	0.1	54.1	33.4	12.3	–	34.8	54.3	10.8
Na-ile	6.7	32.8	60.3	–	6.5	32.7	60.2	–
SiO ₂ -pil-ile	1.3	48.2	50.4	–	0.7	48.0	50.3	–
Mn-SiO ₂ -pil-ile	0.1	46.3	41.5	12.1	–	42.4	46.2	11.4
Cu-SiO ₂ -pil-ile	0.1	46.0	41.3	12.6	–	43.5	46.0	10.5
Fe-SiO ₂ -pil-ile	0.1	45.8	41.1	12.9	–	44.1	45.5	10.4

starting parent material after intercalation process, suggest that the layered structures are preserved. A minor difference in the metal (Cu, Fe and Mn) concentration in bulk (high) and surface (low) composition is observed; this is due to the presence of metal oxide particles inside the layers of ilerite and magadiite.

To verify the existence and chemical environment of the metal oxide species on the catalyst surface, Raman spectral analysis (Fig. S3) for bulk magadiite, ilerite and Cu, Fe and Mn oxides intercalated to SiO₂ pillared magadiite and ilerite samples was performed. A strong band was observed at 465 cm⁻¹ in the Raman spectra of magadiite sample; it was previously reported that the Raman bands in the range of 400–700 cm⁻¹ could assigned to stretching vibration of Si–O–Si modes of six-membered rings of silicon-oxygen tetrahedral units [57]. On other hand, two well separated strong bands at 450 and 480 cm⁻¹ were appeared in the Raman spectrum of bulk ilerite sample. These bands are also attributed to the symmetric stretching vibrational modes of Si-O-Si linkages characteristic of two distinct types of six-membered rings [58]. It is clear that distinct Raman bands were observed in the Raman spectra of ilerite and magadiite samples; therefore, the structure of ilerite is quite different from the magadiite structure.

The Raman spectra of Cu oxide intercalated SiO₂ pillared magadiite and ilerite samples exhibited two additional bands at 290 and 340, cm⁻¹ correspond to CuO phase [59]. It is interesting to observe another additional Raman band at 1120 cm⁻¹, which is not observed in bulk CuO phase, but found in CuO-SiO₂ catalysts due to presence of Cu-O-Si interactive species [60]. The Raman spectra of Fe oxide intercalated SiO₂ pillared magadiite and ilerite samples also showed three additional Raman bands at 330, 495 and 1160 cm⁻¹. These bands are attributed to the framework of Fe-O-Si species. [61]. In other hand, The Raman spectra of Mn oxide intercalated SiO₂ pillared magadiite and ilerite samples exhibited only one new broad Raman band in the range of 640–650 cm⁻¹ was due to a Mn-O mode [62]. These observations clearly indicating that presence of M-O-Si be identified in case Cu and Fe oxide intercalated SiO₂ pillared magadiite and ilerite samples, but the interactive species were not observed in case of Mn oxide intercalated SiO₂ pillared magadiite and ilerite samples.

Fig. S4 shows the nitrogen adsorption-desorption isotherms and pore size distribution patterns (in the inset) for Cu, Fe and Mn oxides intercalated SiO₂ pillared ilerite and magadiite samples. For the sake of comparison, the patterns for bulk SiO₂ pillared samples were also included in the figure. The N₂ adsorption-desorption isotherms of the SiO₂-pillared magadiite and ilerite samples are analogous to a type IV isotherm, distinctive for the mesoporous materials, according to the Brunauer, Deming, Deming and Teller (BDDT) classification [63]. Also, for the ilerite and magadiite samples, the adsorption-desorption isotherms clearly confirm the lack of micropores and the presence of meso- and macropores. As the synthesized ilerite and magadiite normally do not contain large pores, the observed large pores could be due to voids occurred between the crystals of the agglomerates. The hysteresis loop is shown in the isotherms for the SiO₂ pillared materials is of Type H3 as

per the IUPAC classification [64], which is characteristic for the slit-shaped pores due to plate-like particles with voids among the particles [65]. The isotherms of metal intercalated SiO₂ pillared samples exhibited diminutive hysteresis loops and no steps at high relative pressures were observed. This is an indication that the metal oxide intercalated SiO₂ pillared silicates have few external surfaces between the particles. The pore size distribution patterns for all synthesized materials were obtained using NLDFT method (Fig. S4). A typical unimodal pore size distribution curves, in the mesoporous range (above 2 nm), were detected for the SiO₂ pillared samples. The Cu, Fe and Mn oxides intercalated SiO₂ pillared ilerite and magadiite exhibit slightly different pore size distribution compared to parent materials due to the incorporation of large amount of metal oxides resulted a broad range of pore size distribution, demonstrating the development of irregular pore structure. The pore volume and pore width were decreased with intercalation of metal oxides.

The BET surface area observed for Na-ilerite and Na-magadiite were 26 and 21 m² g⁻¹ respectively, however after SiO₂ pillaring the surface area was increased drastically to 582 and 478 m² g⁻¹, which is due to the pillar formation between the silicates layers, similar observations were previously reported by the other researchers [36]. As shown in the Table 2, intercalation of metals in the layered structure altered the porosity of the materials. The metal oxide intercalated SiO₂ pillared materials showed decrease in the BET-surface area. The BET-surface area of Fe oxide intercalated samples is lower compared to Cu and Mn oxides intercalated samples. The formation of highly crystalline Fe and Cu oxide inside and outside of the silicate layers, as evidenced by XRD analysis, could be reason for lower surface area in the Fe and Cu oxides intercalated SiO₂ pillared materials. The decrease in porosity values reveal the metal oxide particles might be located near to edges layers resulting in blockage of interlayers [66].

The H₂-temperature programmed reduction (H₂-TPR) was used for the characterization of layered silicates comprising reducible metal oxides. The reduction of isolated metal oxides, in the layered silicate structure, usually proceeded at lower temperature than that required for the reduction of bulk metal oxides or spinel structures formed due to calcination at higher temperatures [67]. The reduction profile of synthetic SiO₂ pillared magadiite (Fig. 5) displayed no reduction peaks, indicating that the cations presented (Na⁺ and Si⁴⁺) could not be reduced under the experimental conditions selected (25–800 °C). On the other hand, SiO₂ pillared ilerite sample showed low intense noise peaks at around 300 °C and 450 °C, which are not belong to any reducible species, but probably due to complete thermal decomposition of residual CTAB remained in the mesopores of ilerite sample. The Mn oxide intercalated SiO₂ pillared magadiite and ilerite samples showed two different reduction peaks at low temperature region (250–450 °C) and one peak at high temperature region (above 650 °C) with H₂ consumption of 1360 μmol/g and 1618 μmol/g, respectively. These reduction peaks could be associated with the reduction of Mn species via MnO₂ → Mn₃O₄ → MnO [68].

The reduction profiles of Fe intercalated SiO₂ pillared magadiite and

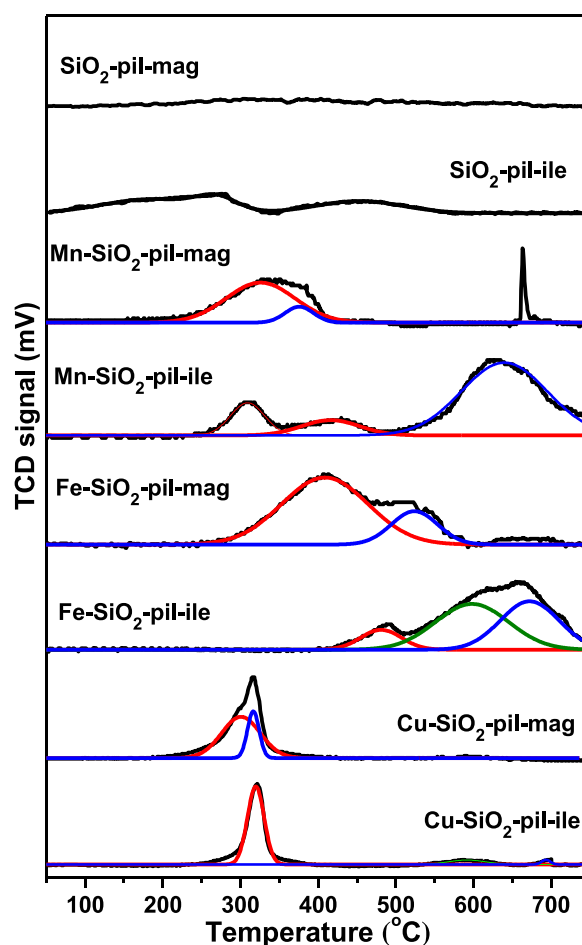


Fig. 5. H₂-TPR patterns of Cu, Fe and Mn oxides intercalated SiO₂-pillared magadiite and ilerite samples.

ilerite samples exhibited three different peaks. It was previously reported in the literature that Fe based catalysts could be reduced via three different steps [69]. The first one corresponds to reduction of Fe₂O₃ to Fe₃O₄ and FeO occurring between 250 °C and 450 °C; subsequently the second one is due to reduction of Fe₃O₄ and FeO to Fe above 500 °C; and third one could be attributed to Fe metal creation from the meta-stable FeO phase. It is clear that the both the samples are following similar trend as reported in the literature. The reduction peaks for Fe oxide intercalated ilerite sample are appeared at higher temperature compared to Fe intercalated magadiite sample; this is possibly due to strong interaction between the Si-O and Fe³⁺ species in ilerite than in the magadiite, as in later sample presence of isolated bulk Fe₂O₃ particles were observed. The Cu intercalated magadiite and ilerite samples showed two reduction peaks at temperature range of 250–350 °C. The TPR peak appear in this range could be attributed to the reduction of Cu²⁺ species [70]. The first reduction peak appeared in the synthesized samples can be assigned to the reduction of isolated CuO species on the surface of silicate layer and the second reduction peak can be attributed to the reduction of CuO interacted with Si-O moieties. The position and intensity of reduction peaks clearly reveal that the fraction of interacted CuO species is high in ilerite compared to magadiite. It is clear that the area of second peak is larger than that of the first peak in case of Cu-SiO₂-pil-ile sample indicating that the relative content of Cu-O-Si species are more in this sample. This is mainly because of ilerite sample able to interact with Cu-O species more effective than magadiite sample and prevented the aggregation of CuO species. The H₂ consumption values for all the synthesized catalysts are tabulated in Table S1, and it is clear that Cu oxide intercalated magadiite and ilerite

Table 2

BET surface area, pore volume and pore width of the synthesized samples.

Catalyst	Surface area (m ² g ⁻¹)	Pore volume (cc g ⁻¹)	Pore width (nm)
SiO ₂ -pil-mag	478	0.426	2.8
Mn-SiO ₂ -pil-mag	392	0.389	2.7
Cu-SiO ₂ -pil-mag	364	0.321	2.5
Fe-SiO ₂ -pil-mag	308	0.285	2.2
SiO ₂ -pil-ile	582	0.521	3.2
Mn-SiO ₂ -pil-ile	488	0.482	3.0
Cu-SiO ₂ -pil-ile	469	0.418	2.7
Fe-SiO ₂ -pil-ile	364	0.382	2.5

catalysts are easily reducible compared to other catalysts and exhibited high H_2 consumption values. It is anticipated that Cu oxide intercalated magadiite and ilerite catalysts could exhibit superior activity in direct catalytic NO decomposition process.

The O_2 -TPD patterns of Cu, Fe and Mn oxides intercalated SiO_2 pillared magadiite and ilerite samples are presented in Fig. 6. It was reported that the oxygen desorption could occur in three stages; The first one at lower temperatures (< 300 °C) could be due to the surface O_2 , O_2^- and O^- species. The second and third stage desorption peaks appear relatively at higher temperatures (< 500 °C), which could be attributed to the release of lattice oxygen of transports from bulk of metal oxide to surface at high temperatures [71]. The both Mn intercalated catalysts exhibited major desorption peaks at high temperatures (greater than 500 °C), which is an indication that they have more of lattice oxygen species. The slight difference in the peak maximum in the magadiite and ilerite could be due to the difference in the particle size, which could retard the release of the bulk lattice oxygen.

It is clear from the figure that the Cu oxide intercalated samples exhibited a sharp major O_2 desorption peak around 400 °C, and two broad desorption peaks at higher temperatures. The major desorption peak at low temperature is indicating the high coverage of molecularly adsorbed O_2 or even the diffusion of O_2 molecules within the silicate layers. Presence of two high temperature O_2 desorption peaks suggesting that two reduction mechanisms are responsible for the evolution of O_2 , as we observed two high-temperature reduction processes in the two samples (H_2 -TPR analysis). It is interesting to note that the Fe intercalated SiO_2 pillared ilerite sample's O_2 -TPD patterns showed two major desorption peaks at low temperatures at 155 °C and 350 °C, and a minor broad peak at 550 °C with a shoulder at 670 °C. The Fe oxide intercalated SiO_2 pillared magadiite sample showed very similar pattern, but the peaks were slightly moved to higher temperatures. Metal oxides

intercalated with SiO_2 pillared ilerite samples can desorb slightly more lattice oxygen than the magadiite samples because their smaller particle size favors the migration of lattice oxygen. The O_2 -TPD spectra of the synthesized samples suggests that Cu and Fe oxides intercalated samples possessed a significant concentration of oxygen species on the catalyst surface at lower temperatures (between of 350 – 450 °C). Meanwhile, in case of Mn oxide intercalated samples, the oxygen desorption started at high temperature (above 400 °C). Moreover, the intensity and area under the sample desorption peak clearly show that Cu oxide intercalated samples' oxygen adsorption capacity is higher compared to Fe and Mn oxides intercalated samples (Table S1).

For direct NO decomposition, the catalytic efficiency of synthesized Cu, Fe and Mn oxides intercalated SiO_2 pillared magadiite and ilerite catalysts were tested. Initially, a blank test was performed without any catalyst and a negligible NO conversion was observed at 400 – 600 °C temperature range under the tested reaction conditions. It is well known that NO usually decomposes into N_2 and O_2 in the direct NO decomposition process [3], but there is a strong possibility of forming unwanted N_2O and NO_2 molecules as side products during the reaction. Different potential catalytic reactions are described below [72].



The influence of reaction temperature in the direct NO decomposition performance over Cu, Fe and Mn oxide intercalated SiO_2 pillared magadiite and ilerite catalysts were studied. It was observed that parent SiO_2 pillared magadiite and ilerite samples exhibited low catalytic activity in the temperature range of 400 – 600 °C. However, the

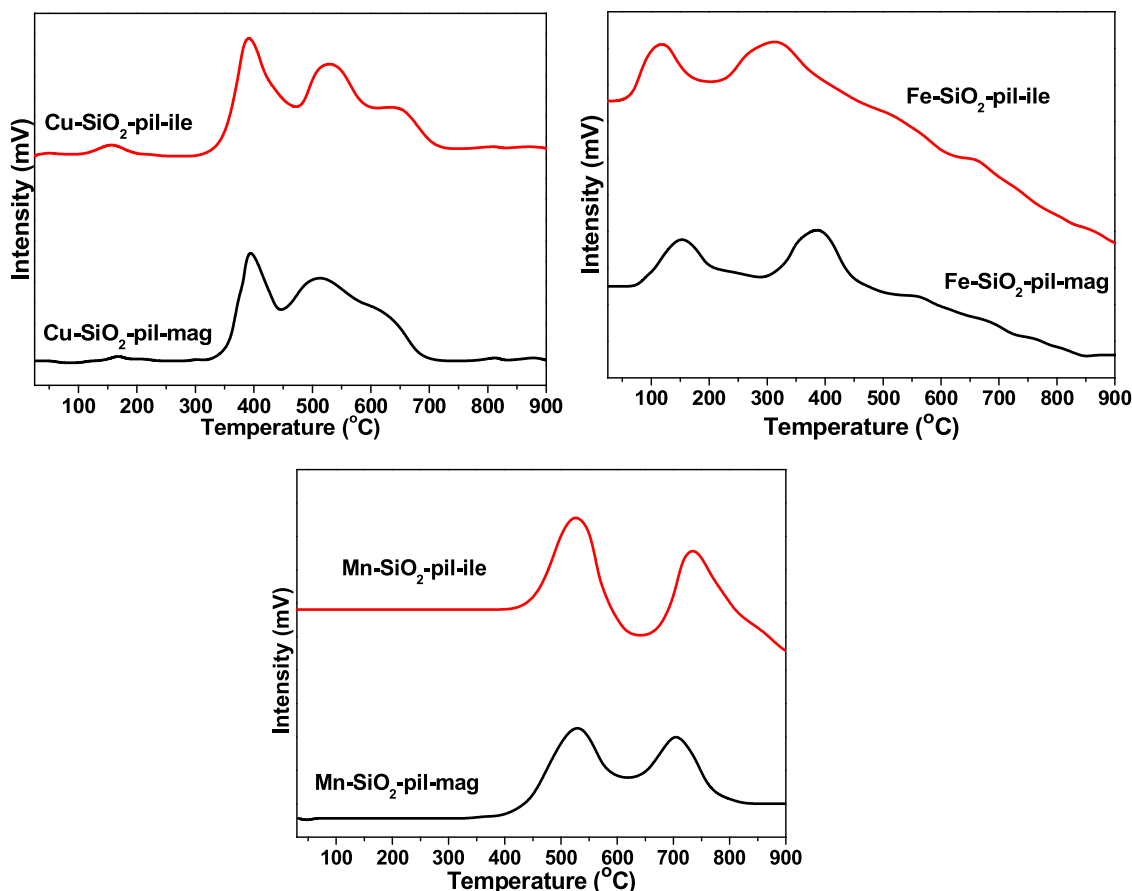


Fig. 6. O_2 -TPD patterns of Cu, Fe and Mn oxides intercalated SiO_2 pillared magadiite and ilerite samples.

intercalation of transition metal (Cu Fe and Mn) oxide resulted in a significant improvement in catalytic activity for direct NO decomposition [Fig. 7 (A)]. A similar observation was reported for CeO₂ supported catalysts that addition of first row transition metals to the CeO₂ support enhanced the direct NO decomposition activity [73]. As shown in the Fig. 7 (A) & (B), with the increase of reaction temperature from 400 °C to 600 °C, both the NO conversion and N₂ selectivity were increased in all transition metal oxide intercalated catalysts.

Among the synthesized samples, the Cu oxide intercalated magadiite and ilerite samples exhibited superior catalytic activity. Intercalation of Fe and Mn oxides to the SiO₂ pillared layered silicates had limited influence on the direct NO decomposition activity at all reaction temperatures. The Cu-SiO₂-pil-ile sample showed NO conversion of 34.4 % at 400 °C and with increase of reaction temperature to 500 °C resulted increase of NO conversion to 73.8 %. It is widely accepted that development of effective catalyst, which could offer high N₂ selectivity and NO conversion is desirable [2]. Interestingly, the synthesized catalysts in this study not yielded any N₂O as a side product under the investigated reaction conditions; the N₂ and NO₂ are the two products detected. It is clear from the stoichiometric reactions that NO₂ is the product which form due to the oxidation of NO, while N₂ is the product due to the direct decomposition of NO.

The N₂ and NO₂ selectivities over the Cu, Fe and Mn oxides intercalated SiO₂ pillared magadiite and ilerite samples at different reaction temperatures are shown in Fig. 7 (B) & (C). The intercalation of Cu oxide led to significant improvement in the N₂ selectivity, as both magadiite and ilerite samples exhibited around 90 % selectivity toward N₂ at 400–500 °C and 85 % selectivity to N₂ at 600 °C. The intercalation of Fe and Mn oxides to the magadiite and ilerite also improved the N₂

selectivity, however these catalysts offered less N₂ selectivity compared to Cu oxide intercalated samples. Interestingly, in case of Fe and Mn oxides intercalated samples; on increase of reaction temperature from 400 to 600 °C resulted in enhancement in selectivity to N₂ from 48 % to 72 % in case Fe-ilerite sample and 40%–65% for Mn-ilerite sample. Intercalation of Cu led to high improvement in N₂ selectivity compared to Fe and Mn oxides intercalation at low reaction temperature. The Mn oxide intercalated samples offered high selectivity to NO₂, probably due to the fact that the mobility of lattice oxygen and the ability of this catalyst to provide the oxygen species to NO molecule to form NO₂ is high.

The Arrhenius plots for NO decomposition for the synthesized catalysts in the temperature range of 400–600 °C are shown in Fig. 8. The apparent activation energy and reaction rate for NO decomposition over most active catalyst; Cu-SiO₂ pillar-ile sample is calculated as 23.2 kcal mol⁻¹ and 2.6 μmol N₂ s⁻¹ g⁻¹ respectively at 500 °C. It was reported that the most active Cu-ZSM-5 catalyst exhibited an activation energy of 22 kcal mol⁻¹ and reaction rate of 12 μmol N₂ s⁻¹ g⁻¹ [74]. For comparison purpose, bulk CuO, α-Fe₂O₃, Mn₂O₃ and SiO₂ supported CuO, α-Fe₂O₃ and Mn₂O₃ samples were tested for the direct NO decomposition. The surface area normalized rates for these catalysts are tabulated in Table S2. It is clear that these samples exhibited very low NO conversion at 400 and 450 °C. The NO conversion rates were increased with increasing the reaction temperature to 500–600 °C. The investigated bulk Cu, Fe, Mn oxides and SiO₂ supported Cu, Fe and Mn oxide samples exhibited lower NO conversions and N₂ selectivity compared to synthesized Cu, Fe and Mn oxide intercalated SiO₂-magadiite and ilerite samples. These observations indicate that the higher direct NO decomposition of metal oxide intercalated layered silicate

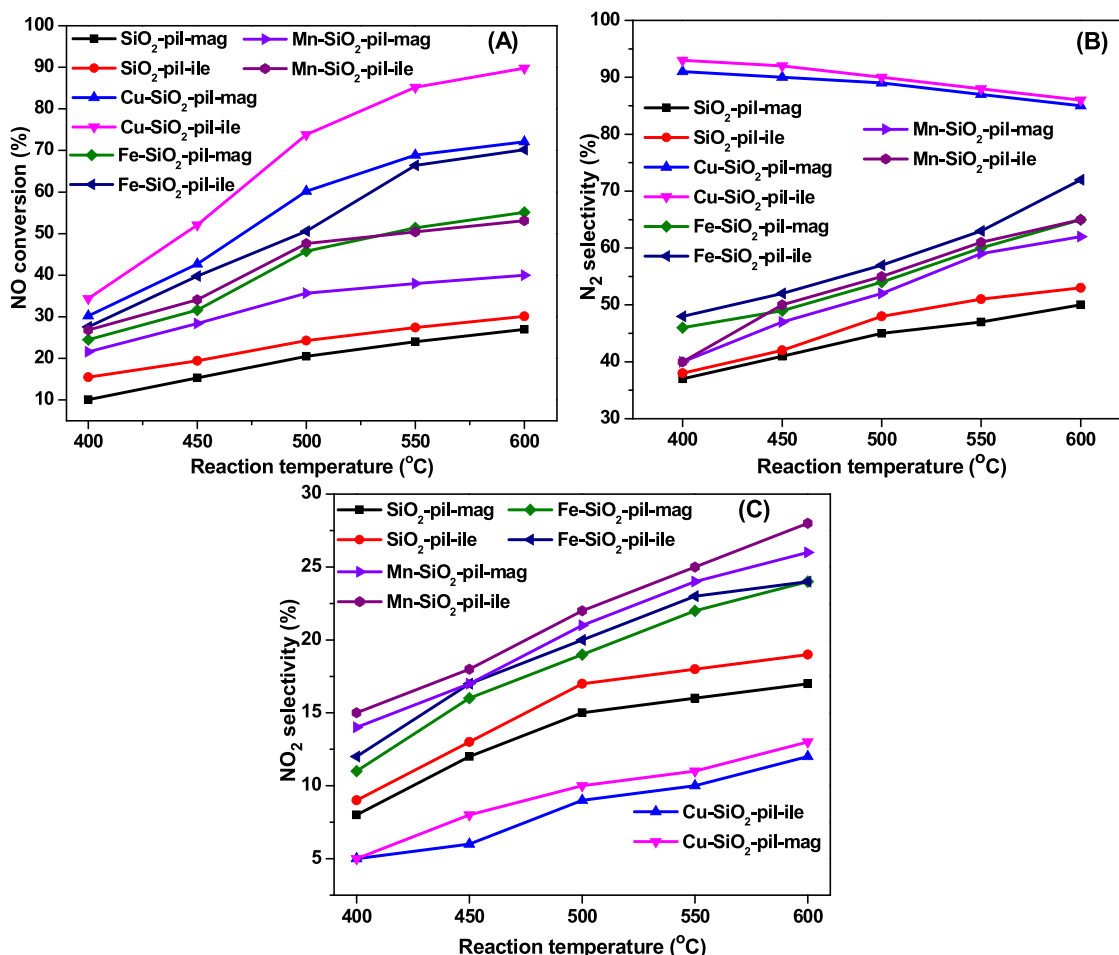


Fig. 7. Influence of reaction temperature on (A) NO conversion (B) N₂ selectivity (C) NO₂ selectivity over synthesized catalysts.

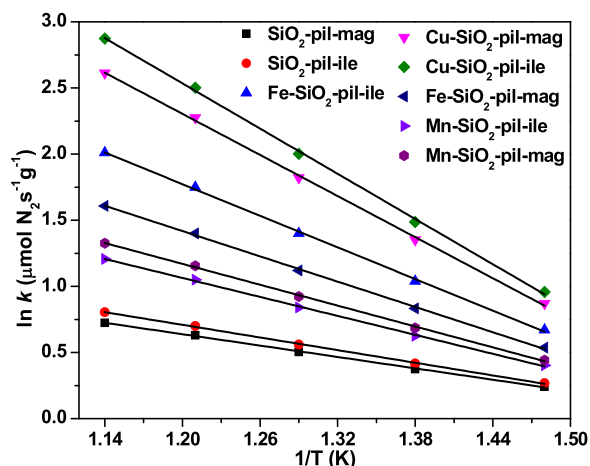


Fig. 8. The Arrhenius plots for NO decomposition for the synthesized catalysts.

samples is not due to aggregated bulk metal oxide on the catalyst surface.

In industrial catalyst development, the catalytic activity at high GHSV is a crucial aspect, therefore the most active catalyst, Cu-SiO₂-pil-ile sample was chosen to study the influence of GHSV on NO decomposition performance and the obtained results are shown in Table 3. With low GHSV, NO decomposition conversions appeared a maximum; gradual increase of GHSV, NO conversion steadily decreased. With the further increase of GHSV to 18,000 h⁻¹, the selectivity to NO₂ has not changed significantly, whereas the selectivity of N₂ steadily increased with the increase of GHSV. This observation reveals that NO conversion to N₂ and NO₂ can be accomplished through separate rate-limiting steps.

It is important to study the mass transport and diffusion limitations for any catalyzed reaction. The external and internal diffusional limitations for the synthesized catalysts in using reported procedures [75] and relevant information is included in the electronic supplementary information. In order to determine the influence of pore diffusion on reaction rate the effectiveness factor 'η' was determined. It is well known that the internal effectiveness factor (η) for a first-order reaction in a spherical catalyst pellet. It was observed that 'η' has value is between 0.95 and 1 for all the investigated catalysts in the present study, therefore there is no internal diffusion resistance is taking place. The influence of external diffusion resistance over the reaction rate is determined by using general diffusion laws, the value of the mass transfer coefficient of reactants and fluid dynamic parameters. It is observed that the calculated k_c values are greater than k for all the catalysts, therefore the NO decomposition proceeds in the kinetic regime and external diffusion is not influencing the NO decomposition rate.

The time on stream analysis (durability of catalyst) is also a significant aspect in catalyst development, and Fig. 9 demonstrates the results of time on stream analysis for Cu-SiO₂-pil-ile sample. It can be seen that the NO conversion and N₂ selectivity were slightly reduced (NO conversion from 89.8% to 85% and N₂ selectivity from 86% to 82%) after continuous operation of 48 h. The slight decrease of activity could be due to sintering of active metal oxide species. The observed formation of NO₂ in the process could be due to the reaction between the

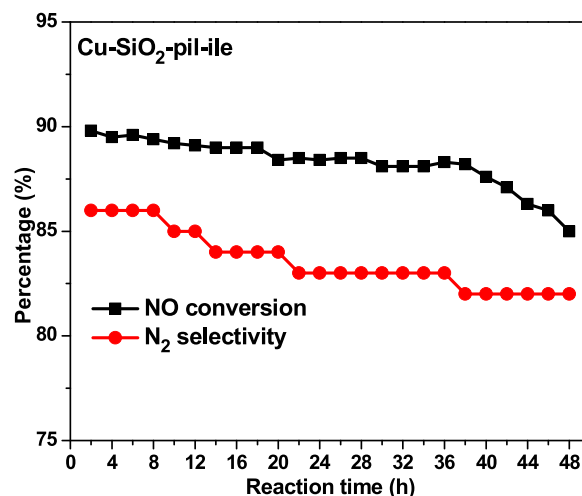


Fig. 9. The time on stream analysis of Cu-SiO₂-pil-ile catalyst.

undecomposed NO with lattice oxygen of the catalyst and this catalytic oxidation appeared be high in case of Mn and Fe oxide intercalated SiO₂ pillared layered silicate samples, a similar observation was reported in case of Cu-Mn oxide catalyst [76]. High NO conversion rates observed in case of Cu, Fe and Mn oxide intercalated layered silicate samples higher reaction temperature could be attributed to high mobility of lattice oxygen, as O₂-TPD patterns of the samples exhibited major desorption peak of lattice oxygen at high temperatures (500–700 °C). Overall, the formation of NO₂ observed with Cu-SiO₂-pil-ile is influenced by lowering the residence time at reaction temperature smaller than 600 °C compared to Fe and Mn oxide intercalated samples.

It was previously reported that the low activity of the catalysts in NO decomposition process could be due to catalyst inability to desorb oxygen formed from NO dissociation [77]. In case of some catalysts, the formed oxygen due to NO dissociation is strongly bounded to surface of catalyst, negatively influencing the active centers and hindering the progression of NO dissociation. The characterization data from XRD, XPS, H₂-TPR and O₂-TPD techniques for Cu, Fe, and Mn intercalated layered silicate samples could be helpful to understand the structure and NO adsorption properties of the investigated samples in this study. Several decades ago, Iwamoto et al. [78] reported that oxygen species adsorbed on Cu²⁺ ions in the aluminosilicates can easily desorb at low temperatures (less than 300 °C), which is the contributing factor for superior activity of the Cu contained aluminosilicates catalysts for NO decomposition. The same research group indicated that large quantity of Cu ions in aluminosilicates could be advantageous to enhance the NO decomposition activity. Later on, Yahiro et al. [79] indicated that Cu⁺ ions in the aluminosilicates generated at high reaction temperatures regarded as active centers and NO decomposition progresses through the creation of NO^{δ-} or (NO)₂^{δ-} species on Cu⁺ species. Groothaert et al. [80] reported that presence of O-bridged Cu planar complexes showed an influence on NO decomposition activity of Cu based catalysts, while Hayes et al. [81] observed that CuO particles are the active catalytic species. Da Costa et al. [82] provided an evidence for the participation of redox cycle of Cu-O-Cu species in NO decomposition activity. The authors also indicated that mobile oxygen atoms in the Cu-O-Cu species are required for rapid redox cycles but not the isolated Cu²⁺ species for NO decomposition. Therefore, it is important to understand the nature of the Cu species in Cu-SiO₂-pil-ile and Cu-SiO₂-pil-mag responsible for the superior catalytic NO decomposition performance.

In the synthesized Cu oxide intercalated layered silicates, majority of Cu is instituted in the form of CuO particles as observed from XRD analysis. It was also observed that the average particle size of CuO was observed as 20 nm, which is too big to move inside the pores of ilerite or magadiite. It is our interpretation that Cu²⁺ ions in CuO particles are at

Table 3

Influence of GHSV on NO conversion, selectivities to N₂ and NO₂ over Cu oxide intercalated SiO₂ pillared ilerite sample.

GHSV (h ⁻¹)	NO conversion (%)	Selectivity to N ₂ (%)	Selectivity to NO ₂ (%)
3000	75.2	88.2	11.0
6000	73.8	90.0	9.0
12,000	61.5	92.1	8.2
18,000	42.9	93.3	7.6
24,000	35.2	94.1	7.1

the interface with SiO₂ pillars of layered silicate surface, as the XPS results clearly indicated that Cu is chemically bonded with Si-O groups in both ilerite and magadiite samples to form an amorphous copper phyllosilicate on the surface. Gong et al. [83] reported that copper phyllosilicates produce stable Cu⁺ species on its surface, which are responsible for hydrogenation reaction.

The H₂-TPR and O₂-TPD results indicated that the Cu-SiO₂-pil-ile and Cu-SiO₂-pil-mag catalysts possessed easily reducible Cu species and mobility of the oxygen atoms is also high, which are directly related to the superior NO decomposition activity. Thus, the activity of Cu-SiO₂-pil-ile and Cu-SiO₂-pil-mag samples could be ascribed to both existence of Cu²⁺ and Cu⁺ species and also to oxygen desorption from Cu species at moderate temperatures. In addition, it is well known that NO is an acidic molecule and the NO adsorption greatly depends on the surface acid/base character of the catalyst. The DRIFT spectra of the pyridine adsorbed catalysts are shown in the Fig. 10 and the Cu-SiO₂-pil-ile and Cu-SiO₂-pil-mag samples possess less number of Lewis and Brønsted acid sites compared with Fe and Mn oxide intercalated samples. This factor is also affecting the reactivity of NO with surface of Cu-SiO₂-pil-ile and Cu-SiO₂-pil-mag catalysts. The current best catalysts for NO decomposition were tabulated in Table S3 (ESI) with the details on the tested reaction temperatures, space velocities, NO conversions and N₂ selectivities. It is clear from the literature review that the multi metal containing perovskite catalysts such as Ba₃Y₃Sc_{0.6}Cu_{0.4}O₉, Ba₃Y_{3.6}-Cu_{0.4}O₉ (700 °C) and zeolite-based catalysts such as Fe/Mel-10@ZSM-5 (350 °C) exhibited high NO decomposition activity compared to the most active catalyst [Cu-SiO₂-pil-ile] in the present study. However, Cu-SiO₂-pil-ile catalyst offered 90 % NO conversion and 83 % N₂ selectivity at 600 °C with very high GHSV value (12,000 h⁻¹) compared to the catalysts reported in the literature. Therefore, it is meaningful to state that the Cu-SiO₂-pi-ile catalyst possessed remarkable NO decomposition activity.

4. Conclusions

In this work, layered silicates (magadiite and ilerite) were pillared with SiO₂ and then intercalated with Cu, Fe and Mn oxides to utilize the synthesized materials as catalysts for direct NO decomposition in the temperature region of 400–600 °C. The catalytic activity results indicated that Cu intercalated SiO₂ pillared magadiite and ilerite samples are efficient catalysts among the synthesized samples (90 % NO conversion and 83 % selectivity to N₂ at 600 °C). Elemental analysis, XRD, FE-SEM, DR UV-vis, Raman spectroscopy, N₂-adsorption, H₂-TPR, O₂-TPD and XPS measurements were used to study the physico-chemical properties of the synthesized metal oxide intercalated layered silicate materials. The results from XRD and N₂ adsorption-desorption

measurements demonstrated that Cu, Fe and Mn oxide-SiO₂ pillared silicate samples possessed different pore structures from SiO₂-pillared silicates, due to the different nature of metal oxides. The Cu-SiO₂-pil-ile and Cu-SiO₂-pil-mag samples possess a smaller number of Lewis and Brønsted acid sites compared with Fe and Mn oxide intercalated samples. The XPS analysis of the samples reveals that intercalation of both Cu and Fe resulted in the presence of Cu²⁺/Cu⁺ and Fe³⁺/Fe²⁺, and the synergism between the redox centers is the major reason for superior performance in NO decomposition. Conversely, Mn remains in single oxidation states (Mn³⁺) in the Mn intercalated catalysts. The H₂-TPR and O₂-TPD results indicated that the Cu-SiO₂-pil-ile and Cu-SiO₂-pil-mag catalysts possessed easily reducible Cu species and mobility of the oxygen atoms is also high, which are directly related to the superior NO decomposition activity. Thus, the activity of Cu-SiO₂-pil-ile and Cu-SiO₂-pil-mag samples could be accredited to both existence of Cu²⁺ and Cu⁺ species and also to oxygen desorption from Cu species at moderate temperatures.

Intellectual property

We confirm that we have given due consideration to the protection of intellectual property associated with this work and that there are no impediments to publication, including the timing of publication, with respect to intellectual property. In so doing we confirm that we have followed the regulations of our institutions concerning intellectual property.

Research ethics

We further confirm that any aspect of the work covered in this manuscript that has involved human patients has been conducted with the ethical approval of all relevant bodies and that such approvals are acknowledged within the manuscript.

Authorship

- 1 Substantial contributions to the conception or design of the work; or the acquisition, analysis, or interpretation of data for the work; AND
- 2 Drafting the work or revising it critically for important intellectual content; AND
- 3 Final approval of the version to be published; AND
- 4 Agreement to be accountable for all aspects of the work in ensuring that questions related to the accuracy or integrity of any part of the work are appropriately investigated and resolved.

All those designated as authors should meet all four criteria for

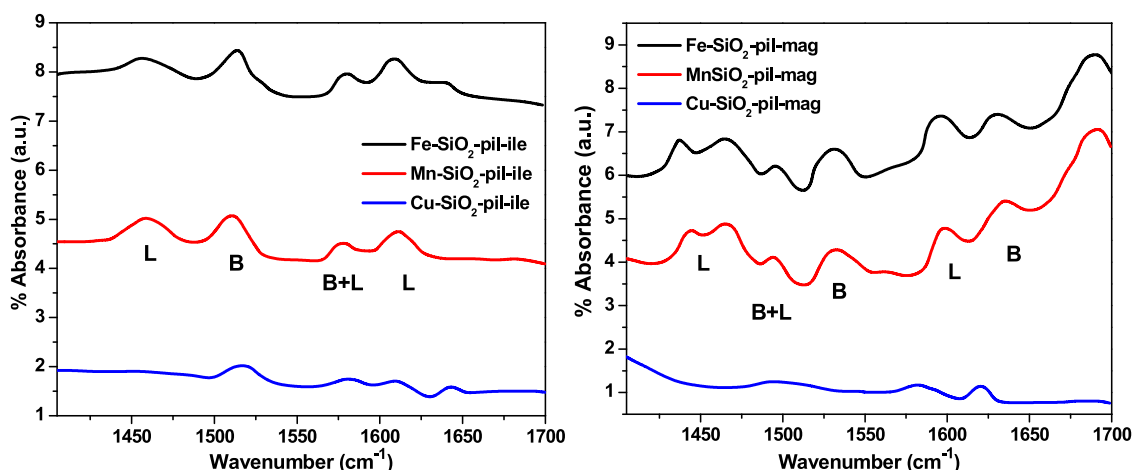


Fig. 10. DRIFT spectra of pyridine adsorbed SiO₂ pillared ilerite and magadiite samples.

authorship, and all who meet the four criteria should be identified as authors. For more information on authorship, please see <http://www.icmje.org/recommendations/browse/roles-and-responsibilities/defining-the-role-of-authors-and-contributors.html#two>

All listed authors meet the ICMJE criteria.

We attest that all authors contributed significantly to the creation of this manuscript, each having fulfilled criteria as established by the ICMJE.

We confirm that the manuscript has been read and approved by all named authors.

We confirm that the order of authors listed in the manuscript has been approved by all named authors

Contact with the editorial office

The Corresponding Author declared on the title page of the manuscript is:

Katabathini Narasimharao.

Funding

This work was funded by the Deanship of Scientific Research (DSR) at King Abdulaziz University, Jeddah, Saudi Arabia under grant no. G-197-130-1440.

CRediT authorship contribution statement

Katabathini Narasimharao: Conceived and designed the research work, collected the data, wrote the paper. **Islam Hamdy Abd El Maksod:** Collected the data, wrote the paper. **Mohamed Mokhtar:** Conceived and designed the research work, collected the data, wrote the paper.

Declaration of Competing Interest

The authors declare no conflict of interest.

Acknowledgements

This project was funded by the Deanship of Scientific Research (DSR) at King Abdulaziz University, Jeddah, under grant no. G-197-130-1440. The authors, therefore, acknowledge with thanks DSR for technical and financial support.

Appendix A. Supplementary data

Supplementary material related to this article can be found, in the online version, at doi:<https://doi.org/10.1016/j.apcata.2021.118100>.

References

- N. Imanaka, T. Masui, Appl. Catal. A Gen. 431-432 (2012) 1-8, <https://doi.org/10.1016/j.apcata.2012.02.047>.
- M. Haneda, H. Hamada, Comptes Rendus Chim. 19 (2016) 1254-1265, <https://doi.org/10.1016/j.crci.2015.07.016>.
- F. Garin, Appl. Catal. A Gen. 222 (2001) 183-219, [https://doi.org/10.1016/S0926-860X\(01\)00827-4](https://doi.org/10.1016/S0926-860X(01)00827-4).
- S. Royer, D. Duprez, F. Can, X. Courtois, C.B. Dupeyrat, S. Laassiri, H. Alamdari, Chem. Rev. 114 (2014) 10292-10368, <https://doi.org/10.1021/cr500032a>.
- J. Zhu, D. Xiao, J. Li, X. Yang, Y. Wu, J. Mol. Catal. A 234 (2005) 99-105, <https://doi.org/10.1016/j.molcata.2005.02.015>.
- H. Iwakuni, Y. Shinmyou, H. Yano, H. Matsumoto, T. Ishihara, Appl. Catal. B 74 (2007) 299-306, <https://doi.org/10.1016/j.apcatb.2007.02.020>.
- N. Imanaka, T. Masui, H. Masaki, Adv. Mater. 19 (2007) 3660-3663, <https://doi.org/10.1002/adma.200602323>.
- W.J. Hong, S. Iwamoto, M. Inoue, Catal. Today 164 (2011) 489-494, <https://doi.org/10.1016/j.cattod.2010.10.063>.
- Y. Teraoka, K. Torigoshi, H. Yamaguchi, T. Ikeda, S. Kagawa, J. Mol. Catal. A 155 (2000) 73-80, [https://doi.org/10.1016/S1381-1169\(99\)00320-9](https://doi.org/10.1016/S1381-1169(99)00320-9).
- S. Matsumoto, Catal. Today 90 (2004) 183-190, <https://doi.org/10.1016/j.cattod.2004.04.048>.
- K. Pacultová, V. Draštková, Ž. Chromčáková, T. Bílková, K.M. Kutláková, A. Kotarba, L. Obalová, Mol. Catal. 428 (2017) 33-40, <https://doi.org/10.1016/j.molcata.2016.11.038>.
- D.K. Lee, Korean J. Chem. Eng. 21 (2004) 611-620, <https://doi.org/10.1007/BF02705495>.
- M.Y. Kustova, S.B. Rasmussen, A.L. Kustov, C.H. Christensen, Appl. Catal. B: Environ. 67 (2006) 60-67, <https://doi.org/10.1016/j.apcatb.2006.04.014>.
- T. Ennaert, J. Van Aelst, J. Dijkmans, R. De Clercq, W. Schutyser, M. Dusselier, D. Verboekend, B.F. Sels, Chem. Soc. Rev. 45 (2016) 584-611, <https://doi.org/10.1039/C5CS00859J>.
- S.J. Kim, K.-D. Jung, O.-S. Joo, E.J. Kim, T.B. Kang, Appl. Catal. A Gen. 266 (2004) 173-180, <https://doi.org/10.1016/j.apcata.2004.02.003>.
- J. Herney-Ramírez, L.M. Madeira, in: A. Gil, S.A. Korili, R. Trujillano, M.A. Vicente (Eds.), Pillared Clays and Related Catalysts, Springer-Verlag, New York, USA, 2010, pp. 129-165, https://doi.org/10.1007/978-1-4419-6670-4_6.
- J. Baloyi, T. Ntho, J. Moma, RSC Adv. 8 (2018) 5197-5211, <https://doi.org/10.1039/C7RA12924F>.
- W. Supronowicz, F. Roessner, W. Schwieger, M. Meilikhov, D. Esken, Clays Clay Miner. 60 (2012) 254-264, <https://doi.org/10.1346/CCMN.2012.0600303>.
- M.E. Landis, B.A. Aufdembrink, P. Chu, I.D. Johnson, G.W. Kirker, M.K. Rubin, J. Am. Chem. Soc. 113 (1991) 3189-3190, <https://doi.org/10.1021/ja00008a067>.
- K. Kosuge, A. Tsunashima, Chem. Commun (1995) 2427-2428, <https://doi.org/10.1039/C39950002427>.
- W. Schwieger, O. Gravenhorst, T. Selvam, F. Roessner, R. Schloegl, D. Su, G.T. P. Mabande, Colloid Polym. Sci. 281 (2003) 584-588, <https://doi.org/10.1007/s00396-002-0835-4>.
- A. Kuhlmann, F. Roessner, W. Schwieger, O. Gravenhorst, T. Selvam, Catal. Today 97 (2004) 303-306, <https://doi.org/10.1016/j.cattod.2004.07.014>.
- W. Schwieger, T. Selvam, O. Gravenhorst, N. Pfaender, R. Schloegl, G.T. P. Mabande, J. Phys. Chem. Solids 65 (2004) 413-420, <https://doi.org/10.1016/j.jpcs.2003.08.032>.
- S.J. Kim, E.J. Kim, T.B. Kang, K.-D. Jung, O.-S. Joo, C.-H. Shin, J. Porous Mater 13 (2006) 27-35, <https://doi.org/10.1007/s10934-006-5487-1>.
- S.-F. Wang, M.-L. Lin, Y.-N. Shieh, Y.-R. Wang, S.-J. Wang, Ceram. Int. 33 (2007) 681-685, <https://doi.org/10.1016/j.ceramint.2005.12.005>.
- S.-H. Ahn, S.-H. Kim, H.-S. Hahm, Res. Chem. Intermed 34 (2008) 793-801, <https://doi.org/10.1007/BF03036940>.
- K. Ozawa, Y. Nakao, Z. Cheng, D. Wang, M. Osada, R. Okada, Mater. Lett. 63 (2009) 366-369, <https://doi.org/10.1016/j.matlet.2008.10.038>.
- A. Gil, M.A. Vicente, S.A. Korili, Catal. Today 112 (2006) 117-120, <https://doi.org/10.1016/j.cattod.2005.11.046>.
- Z. Ding, J.T. Klopogge, R.L. Frost, J. Porous Mater 8 (2001) 273-293, <https://doi.org/10.1023/A:1013113030912>.
- A. Świąć, A. Kowalczyk, M. Rutkowska, U. Dfiaz, A.E. Palomares, L. Chmielarz, Catalysts 10 (7) (2020) 734, <https://doi.org/10.3390/catal10070734>.
- U. Brenn, H. Ernst, D. Freude, R. Herrmann, R. Jähnig, H.G. Karge, J. Kärger, T. König, B. Mädlar, U.-T. Pingel, D. Prochnow, W. Schwieger, Microporous Mesoporous Mater. 40 (2000) 43-52, [https://doi.org/10.1016/S1387-1811\(00\)00241-9](https://doi.org/10.1016/S1387-1811(00)00241-9).
- K. Narasimharao, A. Alshehri, Fuel 278 (2020) 118375, <https://doi.org/10.1016/j.fuel.2020.118375>.
- G.L. Paz, E.C.O. Munsignatti, H.O. Pastore, J. Mol. Catal. A Chem. 422 (2016) 43-50, <https://doi.org/10.1016/j.molcata.2016.02.014>.
- A.O. Moura, A.G.S. Prado, J. Colloid Interface Sci. 330 (2009) 392-398, <https://doi.org/10.1016/j.jcis.2008.10.032>.
- K. Kosuge, P.S. Singh, Chem. Mater. 12 (2000) 421-427, <https://doi.org/10.1021/cm990451m>.
- S. Vortmann, J. Rius, S. Siegmann, H. Gies, J. Phys. Chem. B 101 (1997) 1292-1297, <https://doi.org/10.1021/jp962162g>.
- W. Lim, J.-H. Jang, N.-Y. Park, S.-M. Paek, W.-C. Kim, M. Park, J. Mater. Chem. A 5 (2017) 4144-4149, <https://doi.org/10.1039/C7TA00038C>.
- D. Sebag, E.P. Verrecchia, S.-J. Lee, A. Durand, Sediment. Geol. 139 (2001) 15-31, [https://doi.org/10.1016/S0037-0738\(00\)00152-4](https://doi.org/10.1016/S0037-0738(00)00152-4).
- T. Iwasaki, T. Kuroda, S. Ichio, M. Satoh, Chem. Eng. Comm. 193 (2006) 69-76, <https://doi.org/10.1080/009864490923529>.
- Q. Wang, Y. Zhang, T. Hu, X. Jing, C. Meng, Microporous Mesoporous Mater. 246 (2017) 102-113, <https://doi.org/10.1016/j.micromeso.2017.03.024>.
- Y. Chen, G. Yu, F. Li, J. Wei, Appl. Clay Sci. 88 (2014) 163-169, <https://doi.org/10.1016/j.clay.2013.12.014>.
- I.R. Iznaga, V. Petranovskii, G.R. Fuentes, C. Mendoza, A.B. Aguilar, J. Colloid Interface Sci. 316 (2) (2007) 877-886, <https://doi.org/10.1016/j.jcis.2007.06.021>.
- K. Wang, L. Yang, W. Zhao, L. Cao, Z. Sun, F. Zhang, Green Chem. 19 (2017) 1949-1957, <https://doi.org/10.1039/C7CG00219J>.
- Y. Liu, C. Dong, H. Wei, W. Yuan, K. Li, Appl. Clay Sci. 118 (2015) 301-307, <https://doi.org/10.1016/j.clay.2015.10.010>.
- S.A. Kulkarni, P.S. Sawadh, P.K. Palei, J. Korean Chem. Soc. 58 (2014) 100-104, <https://doi.org/10.5012/jkcs.2014.58.1.100>.
- C. Hui, C. Shen, J. Tian, L. Bao, H. Ding, C. Li, Y. Tian, X. Shi, H.-J. Gao, Nanoscale 3 (2011) 701-705, <https://doi.org/10.1039/C0NR00497A>.
- Y. Omomo, T. Sasaki, L. Wang, M. Watanabe, J. Am. Chem. Soc. 125 (2003) 3568-3575, <https://doi.org/10.1021/ja021364p>.
- D. Radu, P. Glatzel, A. Glotter, O. Stephan, B.M. Weckhuysen, F.M.F. de Groot, J. Phys. Chem. C 112 (2008) 12409-12416, <https://doi.org/10.1021/jp802915k>.

- [49] J.J. Chambers, G.N. Parsons, *J. Appl. Phys.* 90 (2001) 918–933, <https://doi.org/10.1063/1.1375018>.
- [50] M.J. Guittet, J.P. Crocombette, M. Gautier-Soyer, *Phys. Rev. B* 63 (2001) 125117, <https://doi.org/10.1103/PhysRevB.63.125117>.
- [51] X.M. Huang, M. Ma, S. Miao, Y.P. Zheng, M.S. Chen, W.J. Shen, *Appl. Catal. A Gen.* 531 (2017) 79–88, <https://doi.org/10.1016/j.apcata.2016.12.006>.
- [52] A.P. Grosvenor, B.A. Kobe, M.C. Biesinger, N.S. McIntyre, *Surf. Interface Anal.* 36 (2004) 1564–1574, <https://doi.org/10.1002/sia.1984>.
- [53] A.K. Shukla, P. Krüger, R.S. Dhaka, D.I. Sayago, K. Horn, S.R. Barman, *Phys. Rev. B* 75 (2007) 235419, <https://doi.org/10.1103/PhysRevB.75.235419>.
- [54] H.W. Nesbitt, S.B. Banerjee, *Am. Mineral.* 83 (1998) 305–315, <https://doi.org/10.2138/am-1998-3-414>.
- [55] Y. Du, M.-S. Zhang, J. Hong, Y. Shen, Q. Chen, Z. Yin, *Appl. Phys. A* 76 (2003) 171–176, <https://doi.org/10.1007/s003390201404>.
- [56] Z. Wang, T.J. Pinnavaia, *J. Mater. Chem.* 13 (2003) 2127–2131, <https://doi.org/10.1039/B306167A>.
- [57] J.M. Garcés, S.C. Rocke, C.E. Crowder, D.L. Hasha, *Clays Clay Miner.* 36 (1988) 409–418, <https://doi.org/10.1346/CCMN.1988.0360505>.
- [58] Y. Huang, Z. Jiang, W. Schwieger, *Chem. Mater.* 11 (1999) 1210–1217, <https://doi.org/10.1021/cm980403m>.
- [59] W. Wang, Z. Liu, Y. Liu, C. Xu, C. Zheng, G. Wang, *Appl. Phys. A* 76 (2003) 417–420, <https://doi.org/10.1007/s00339-002-1514-5>.
- [60] H. Li, L. Ban, Z. Wang, P. Meng, Y. Zhang, R. Wu, Y. Zhao, *Nanomaterials* 9 (2019) 842, <https://doi.org/10.3390/nano9060842>.
- [61] F. Fan, Z. Feng, C. Li, *Acc. Chem. Res.* 43 (2010) 378–387, <https://doi.org/10.1021/ar900210g>.
- [62] F. Buciuman, F. Patcas, R. Craciun, D.R.T. Zahn, *Phys. Chem. Chem. Phys.* 1 (1999) 185–190, <https://doi.org/10.1039/A807821A>.
- [63] J.P. Nguetnkam, R. Kamga, F. Villieras, G.E. Ekodeck, A. Razafitianamaharavo, J. Yvon, *J. Colloid Interf. Sci.* 289 (2005) 104–115, <https://doi.org/10.1016/j.jcis.2005.03.053>.
- [64] K.S.W. Sing, *Pure Appl. Chem.* 54 (1982) 2201–2218, <https://doi.org/10.1351/pac198254112201>.
- [65] O. Barth, J. Kornatowski, J.A. Lercher, *J. Mater. Chem.* 12 (2002) 369–373, <https://doi.org/10.1039/B104824B>.
- [66] D. Dutta, B.J. Borah, L. Saikia, M.G. Pathak, P. Sengupta, D.K. Dutta, *Appl. Clay Sci.* 53 (2011) 650–656, <https://doi.org/10.1016/j.clay.2011.05.018>.
- [67] V. Rives, M. A. Ulibarri, A. Montero, *Appl. Clay Sci.* 10 (1995) 83–93, [https://doi.org/10.1016/0169-1317\(95\)00009-S](https://doi.org/10.1016/0169-1317(95)00009-S).
- [68] O. Ostrovski, N. Anacleto, S. Ganguly, *Reduction of Manganese Ores by Methane Containing Gas, Proceedings Tenth International Ferroalloys Congress, 173-183, 2004. ISBN: 0-9584663-5-1.*
- [69] K. Keyvanloo, B. Huang, T. Okeson, H.H. Hamdeh, W.C. Hecker, *Catalysts* 8 (2018) 77, <https://doi.org/10.3390/catal8020077>.
- [70] L. Lin, P.B. Pan, Z.F. Zhou, *Chin. J. Catal.* 32 (2011) 957–968, [https://doi.org/10.1016/S1872-2067\(10\)60223-9](https://doi.org/10.1016/S1872-2067(10)60223-9).
- [71] Y.G. Zhang, Z.F. Qin, G.F. Wang, H.Q. Zhu, M. Dong, S.N. Li, Z.W. Wu, Z.K. Li, Z. H. Wu, J. Zhang, T.D. Hu, W.B. Fan, J.G. Wang, *Appl. Catal. B: Environ.* 129 (2013) 172–181, <https://doi.org/10.1016/j.apcatb.2012.09.021>.
- [72] Q. Sun, Z. Wang, D. Wang, Z. Hong, M. Zhou, X. Li, *Catal. Sci. Technol.* 8 (2018) 4563–4575, <https://doi.org/10.1039/C8CY01114A>.
- [73] G.K. Reddy, T.C. Peck, C.A. Roberts, *J. Phys. Chem. C* 123 (47) (2019) 28695–28706, <https://doi.org/10.1021/acs.jpcc.9b07736>.
- [74] Y. Li, W.K. Hall, *J. Catal.* 129 (1991) 202–215, [https://doi.org/10.1016/0021-9517\(91\)90024-X](https://doi.org/10.1016/0021-9517(91)90024-X).
- [75] R. Tesser, E. Santacesaria, *Processes* 8 (2020) 1599, <https://doi.org/10.3390/pr8121599>.
- [76] T. Liu, Y. Yao, L. Wei, Z. Shi, L. Han, H. Yuan, B. Li, L. Dong, F. Wang, C. Sun, *J. Phys. Chem. C* 121 (23) (2017) 12757–12770, <https://doi.org/10.1021/acs.jpcc.7b02052>.
- [77] K. Almusaiter, R. Krishnamurthy, S.S.C. Chuang, *Catal. Today* 55 (2000) 291–299, [https://doi.org/10.1016/S0920-5861\(99\)00242-4](https://doi.org/10.1016/S0920-5861(99)00242-4).
- [78] M. Iwamoto, S. Yokoo, K. Sasaki, S. Kagawa, *J. Chem. Soc. Faraday Trans. 1* (77) (1981) 1629–1638, <https://doi.org/10.1039/F19817701629>.
- [79] H. Yahiro, M. Iwamoto, *Appl. Catal. A Gen.* 222 (2001) 163–181, [https://doi.org/10.1016/S0926-860X\(01\)00823-7](https://doi.org/10.1016/S0926-860X(01)00823-7).
- [80] M.H. Groothaert, J.A. van Bokhoven, A.A. Battiston, B.M. Weckhuysen, R. A. Schoonheydt, *J. Am. Chem. Soc.* 125 (2003) 7629–7640, <https://doi.org/10.1021/ja029684w>.
- [81] N.W. Hayes, R.W. Joyner, E.S. Shpiro, *Appl. Catal. B: Environ.* 8 (1996) 343–363, [https://doi.org/10.1016/0926-3373\(95\)00074-00077](https://doi.org/10.1016/0926-3373(95)00074-00077).
- [82] P. Da Costa, B. Moden, G.D. Meitzner, D. Ki Leeza, E. Iglesia, *Phys. Chem. Chem. Phys.* 4 (2002) 4590–4601, <https://doi.org/10.1039/B203700A>.
- [83] J. Gong, H. Yue, Y. Zhao, S. Zhao, L. Zhao, J. Lv, S. Wang, X. Ma, *J. Am. Chem. Soc.* 134 (2012) 13922–13925, <https://doi.org/10.1021/ja3034153>.